

Review

# Engineering of GH11 Xylanases for Optimal pH Shifting for Industrial Applications

In Jung Kim <sup>1,\*</sup>, Soo Rin Kim <sup>2</sup> , Uwe T. Bornscheuer <sup>3</sup>  and Ki Hyun Nam <sup>4,\*</sup> 

- <sup>1</sup> Department of Food Science & Technology, Institute of Agriculture and Life Science, Gyeongsang National University, Jinju 52828, Republic of Korea
- <sup>2</sup> School of Food Science and Biotechnology, Kyungpook National University, Daegu 41566, Republic of Korea; soorinkim@knu.ac.kr
- <sup>3</sup> Department of Biotechnology and Enzyme Catalysis, Institute of Biochemistry, University of Greifswald, Felix-Hausdorff-Str. 4, 17489 Greifswald, Germany; uwe.bornscheuer@uni-greifswald.de
- <sup>4</sup> College of General Education, Kookmin University, Seoul 02707, Republic of Korea
- \* Correspondence: ij0308@gnu.ac.kr (I.J.K.); structure@kookmin.ac.kr (K.H.N.)

**Abstract:** Endo-1,4- $\beta$ -xylanases belonging to the glycoside hydrolase (GH) 11 family hydrolyze the  $\beta$ -1,4-glycosidic linkages in the xylan backbone to convert polymeric xylan into xylooligosaccharides. GH11 xylanases play an essential role in sugar metabolism and are one of the most widely used enzymes in various industries, such as pulp and paper, food and feed, biorefinery, textile, and pharmaceutical industries. pH is a crucial factor influencing the biochemical properties of GH11 xylanase and its application in bioprocessing. For the optimal pH shifting of GH11 xylanase in industrial applications, various protein engineering studies using directed evolution, rational engineering, and in silico approaches have been adopted. Here, we review the functions, structures, and engineering methods developed for the optimal pH shifting of GH11 xylanases. The various GH11 engineering techniques and key residues involved in pH shifting are discussed based on their crystal and modeled structure. This review provides an overview of recent advancements in the characterization and engineering of GH11 xylanases, providing a guide for future research in this field.

**Keywords:** xylanase; GH11; engineering; pH; tolerance; structure



**Citation:** Kim, I.J.; Kim, S.R.; Bornscheuer, U.T.; Nam, K.H. Engineering of GH11 Xylanases for Optimal pH Shifting for Industrial Applications. *Catalysts* **2023**, *13*, 1405. <https://doi.org/10.3390/catal13111405>

Academic Editors: Rosa María Oliart-Ros and María Guadalupe Sánchez-Otero

Received: 19 September 2023  
Revised: 24 October 2023  
Accepted: 27 October 2023  
Published: 30 October 2023



**Copyright:** © 2023 by the authors. Licensee MDPI, Basel, Switzerland. This article is an open access article distributed under the terms and conditions of the Creative Commons Attribution (CC BY) license (<https://creativecommons.org/licenses/by/4.0/>).

## 1. Introduction

Xylan is the major constituent of hemicellulose in plant cell walls [1]. It has a complex and heterogeneous structure with a linear chain composed of xylose units linked together via  $\beta$ -1,4 glycosidic bonds [2]. The xylose backbone is variably substituted with a range of sugars and/or organic acids, restricting the accessibility of the enzyme to the target site. Endo-xylanases (EC 3.2.1.8) randomly hydrolyze the  $\beta$ -1,4 glycosidic linkages in the xylan backbone, converting the polymeric xylan into xylooligosaccharides with different degrees of polymerization and the xylose monomer [3]. Chemical and structural information on glycoside hydrolases (GHs) associated with xylanases is available in the carbohydrate-active enzyme database (CAZy). This database classifies relevant enzymes based on sequence similarity [4]. The major GH families associated with xylanase are 5, 7, 8, 9, 10, 11, 12, 16, 26, 30, 43, 44, 51, and 62 [5]. Enzymes in GH families 5, 7, 8, 10, 11, and 43 have a single distinct catalytic domain, whereas those in GH families 16, 51, and 62 have two catalytic domains with bifunctional properties [6]. Enzymes in GH families 9, 12, 26, 30, and 44 have secondary xylanolytic action. Moreover, according to the CAZy database, most endo-xylanases belong to GH families 10 and 11. Although the GH11 family is considered the only “true xylanase” family that has high specificity and selectivity toward xylan substrates, it lacks cellulase or xylosidase activity [7–9]. GH11 xylanases have high application value owing to their catalytic activity and broad temperature/pH spectra [10].

Xylanases are used as biocatalysts in multiple industrial fields, including the paper/pulp, food/feed, textile, chemical/pharmaceutical, and biorefinery industries [11,12] (Figure 1). During the bleaching of Kraft pulp in the paper industry, the lignin in wood chips is removed through sequential treatment with chlorine, chlorine dioxide, and NaOH [13]. Chlorine and chlorine dioxide generate persistent organic chemicals that are toxic to organisms and pose risks to human health. The pretreatment of paper pulp with xylanases increases the chemical lignin extraction efficiency and reduces the amount of chlorine and chlorine dioxide required for extraction. Therefore, xylanases are frequently used for the biobleaching of pulp, thereby improving final paper quality [11]. In the food industry, xylanases can be added to baking dough to improve the quality of baking products by enhancing gluten elasticity, texture, and moisture content [14]. In the feed industry, xylanases are applied as feed ingredients to improve digestibility and produce bioactive prebiotic xylooligosaccharides [15]. In biorefinery, lignocellulosic biomass is converted to various industrially valuable materials, including sugars, fuels, and chemicals [16]. Xylanases are further involved in the saccharification process of lignocellulose biorefinery, contributing to the production of fermentable sugars [17].

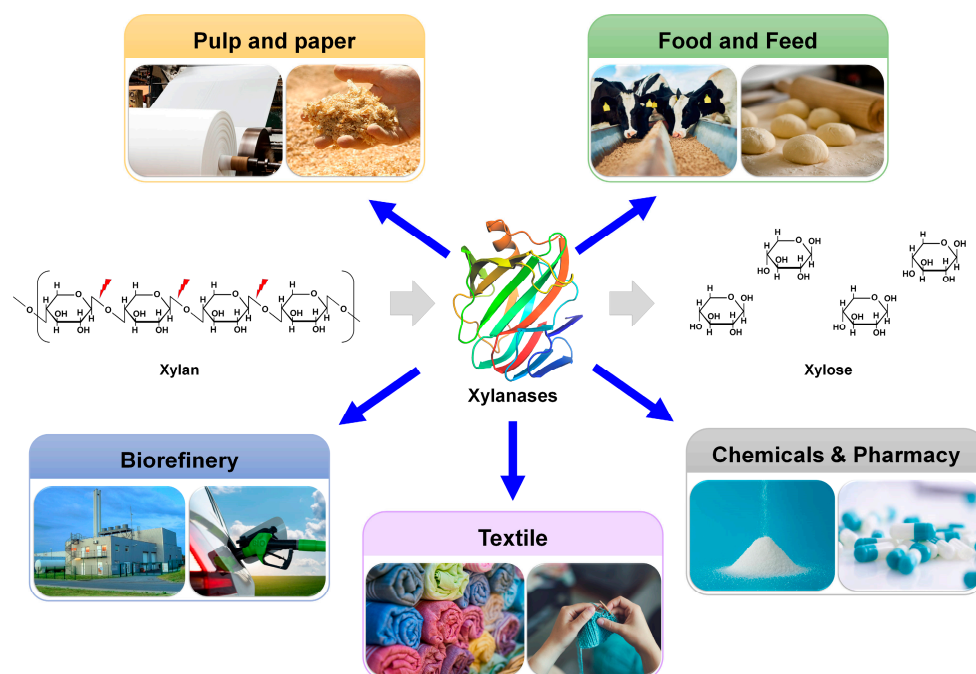


**Figure 1.** Industrial application of xylanases.

GH11 xylanases are highly desirable for these industrial applications, particularly because they lack cellulase activity. These bioprocesses often require extreme conditions in terms of pH, temperature, and inhibitors [14,17]. For example, pulp bleaching involves heat (70 °C) and alkalinity (pH > 9), requiring thermoalkaline enzymes [14]. In biotechnological processes, such as baking, fruit juice clarification, or xylo-oligosaccharides production, xylanases with high activity at acidic pH are preferred [11,18]. When using yeast that expresses xylanase for cellulosic ethanol production, enzymes that are tolerant to toxic solvents, such as ethanol and acetate, are preferred [19,20].

Protein engineering is a multidisciplinary scientific field that focuses on protein design, modification, and optimization to improve their characteristics or achieve specific functions [21]. Protein engineering, guided by directed evolution (DE) and (semi)rational engineering, has emerged as a potent technology with the potential to advance the biotechnology era [22]. Powered by recent outstanding advancements in artificial intelligence (AI) technologies, AlphaFold, a cutting-edge AI system developed by DeepMind, has revolutionized structural biology by rapidly and accurately predicting the 3D structure of a

protein directly from its amino acid sequence [23]. It can provide a wealth of structural information and enhance our understanding of the structural basis of protein function. Thus, it enables researchers to make more informed decisions in the design and modification of proteins. Moreover, AI-assisted powerful tools for designing and creating high-quality and new proteins de novo have been recently developed, exemplified by ProteinMPNN [24].

Xylanases with high activity and stability under extreme conditions have been screened from various extremophiles or developed based on DE or rational design (RD)-guided protein engineering [25–29]. However, there is limited information on semi-RD-based xylanase engineering, which often involves computational prediction followed by site-saturation mutagenesis. Particularly, xylanases belonging to the GH11 family are mostly sourced from non-extremophiles [30] and require engineering to become suitable for harsh bioprocessing conditions.

The temperature and pH-related biochemical properties of GH11 xylanases are important factors to consider to achieve a feasible and eco-friendly bioprocess. In particular, by shifting the optimal pH, altering the pH profile, and ensuring pH stability, these enzymes can effectively carry out their intended functions, leading to improved efficiency in various relevant industrial processes. To engineer the pH-associated features of GH11 enzymes, various strategies, such as site-directed mutagenesis [31,32], RD, modeling/site-directed mutagenesis, structural comparison, redesign of electrostatic potential [33], structure analysis [34,35], and bioinformatics- and biostatistics-based approaches [36], have been used. In a recent review, comprehensive up-to-date strategies for creating a diverse xylanase gene library; implementing high-throughput systems to screen enhanced xylanase mutants derived by DE; and utilizing in silico methods for the prediction based on, for example, Framework for Rapid Enzyme Stabilization by Computational libraries (FRESKO) and in-depth analysis of target mutations were thoroughly examined [37] to obtain desirable industrial characteristics, such as alkaliphilic enhancement, thermal stability, and catalytic performance. Nevertheless, protein engineering studies that involve altering the pH profile and improving pH stability are relatively scarce compared with the efforts put into engineering temperature-related properties, such as improving xylanase thermostability. Furthermore, to date, there is no systematic review on this topic.

In this review, we examine the molecular functions and structures of GH11 xylanases and provide a detailed analysis of important pH profile engineering studies on GH11 xylanases. This is, to the best of our knowledge, the first review on protein engineering of GH11 xylanases for optimal pH shifting, which is important for further industrial applications. The various cases of optimal pH shifting and structural analysis results in this review could provide important insights, facilitating the enzyme engineering of industrial xylanase with optimal pH-shifting characteristics.

## 2. Functions and Structures of GH11 Xylanases

### 2.1. Catalytic Mechanisms

Hydrolysis by GHs occurs through a retaining or inverting mechanism [38]. Enzymatic hydrolysis by GH family members requires two acidic residues (glutamate (Glu) or aspartic acid (Asp)) to act as a proton donor and nucleophile/base, respectively [38]. The GH11 family utilizes a retention mechanism catalyzed by two conserved Glu residues. Xyl-11 from *Bacillus* sp. KT12 is the most widely used model for the GH11 catalytic mechanism investigation. The history of the catalytic mechanism of Xyl-11 identification is well documented [7].

The two catalytic Glu residues of Xyl-11 catalyze a double-displacement mechanism involving a covalent glycosyl enzyme intermediate [39–41]. The retaining mechanism of GH11 can be divided into two main steps: glycosylation and deglycosylation (Figure 2). In the first step (glycosylation), the acid–base Glu residue acts as an acid and protonates the substrate. The nucleophile Glu residue facilitates the departure of the leaving group and the formation of the  $\alpha$ -glycosyl enzyme intermediate during the oxocarbenium-ion-like transition state. In the second step (deglycosylation), the acid–base Glu residue acts

as a base and abstracts a proton from a water molecule. Subsequently, the molecule attacks the anomeric carbon of the  $\alpha$ -glycosyl enzyme intermediate. Furthermore, a second substitution occurs, where the anomeric carbon produces a product with the  $\beta$  configuration identical to that of the substrate (Figure 2).

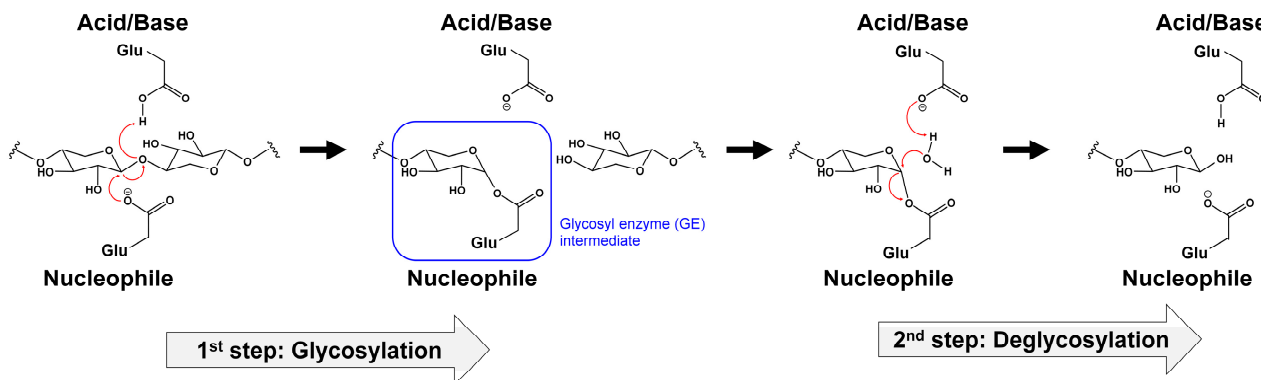


**Figure 2.** Retaining catalytic mechanism of GH11 xylanase with double-displacement of two glutamate residues.

This traditionally identified retaining mechanism of GH11 xylanases is consistent with recent computational analysis findings. This analysis used ab initio quantum mechanics/molecular mechanics calculations with a neutron crystal structure that supported the glycosylation reaction mechanism steps. It revealed the protonation states of the residues involved in the reaction mechanism [42].

## 2.2. Structures

To date, more than 100 GH11 xylanase structures from various organisms have been deposited in the Protein Data Bank (PDB) (<https://www.rcsb.org/>, accessed on 9 August 2023). Representative crystal structures of GH11 xylanases from various organisms are listed in Table 1.

**Table 1.** Xylanase GH11 xylanase structures.

Accession No.	Source Organism	GENE NAME	PDB Code (Complexed Ligand, Mutation)
P36217	<i>Trichoderma reesei</i> ( <i>Hypocrea jecorina</i> ) or <i>Trichoderma reesei</i> RUT C-30	<i>Endo-1,4-<math>\beta</math>-xylanase 2</i> ( <i>xyn2</i> )	1ENX, 1XYN, 1XYO, 1XYP, 1RED (4,5-epoxy pentyl beta-D-xyloside), 1REE (3,4-epoxybutyl beta-D-xyloside), 1REF (2,3-epoxypropyl beta-D-xyloside), 2D97, 2D98, 2DFB, 2DFC, 3LGR (2,6-pyridinedicarboxylic acid), 4HK8 (xylohexaose), 4HK9 (xylotriase), 4HKL, 4HKO, 4HKW, 4S2D (MES), 4S2F, 4S2G, 4S2H, 4XQ4, 4XQD, 4XQW, 4XPV, 5K7P, 5ZF3 (xylotriase), 5ZH0, 5ZH9 (Y88F), 5ZII (xylotriase, Y88F), 5ZIW (Y77F), 5ZKZ (xylotriase, Y77F), 5ZO0, 6JUG (xylotriase), 6JWB (xylotriase), 6JXL (xylotriase), 6JZP (xylotriase), 6K9O, 6K9R (xylotriase), 6KW9 (xylotriase), 6KWD (xylotriase), 6KWF (xylotriase), 6KWG (xylotriase), 6K9W (xylotriase), 6KWC, 6K9X (xylotriase), 6KVV (xylotriase), 6KWE, 6KWH (xylotriase)
P09850	<i>Niallia circulans</i> ( <i>Bacillus circulans</i> )	<i>Endo-1,4-<math>\beta</math>-xylanase</i> ( <i>xlnA</i> )	2BVV, 1BVV, 1C5H, 1C5I, 1HV0, 1HV1, 3VZJ, 3VZK, 3VZL, 3VZM (2-deoxy-2-fluoro-xylobiose), 3VZN (2-deoxy-2-fluoro-xylobiose), 3VZO (2-deoxy-2-fluoro-xylobiose)
P18429	<i>Bacillus subtilis</i> (strain 168)	<i>Endo-1,4-<math>\beta</math>-xylanase A</i> ( <i>xynA</i> )	1XXN, 2DCY, 2DCZ, 2B42 ( <i>Triticum xylanase inhibitor-IA</i> ), 2B45, 2B46, 2QZ3 (xylotetraose), 2Z79, 3HD8 ( <i>Triticum aestivum xylanase inhibitor-IIA</i> ), 3EXU,
A0A7G1MBT0	<i>Streptomyces olivaceoviridis</i> ( <i>Streptomyces corchorusii</i> )	<i>Endo-1,4-<math>\beta</math>-xylanase</i>	7DFM, 7DFN ( $\alpha$ -L-arabinofuranosyl xylotriase), 7DFO (4-O-methyl- $\alpha$ -D-glucuronopyranosyl xylotriase)
P55329	<i>Aspergillus niger</i>	<i>Endo-1,4-<math>\beta</math>-xylanase A</i> ( <i>xynA</i> )	1T6G, 2QZ2 (xylopentaose), 6QE8 (xylobiose epoxide)

GH11 xylanases have a  $\beta$ -jelly roll structure consisting of two antiparallel  $\beta$ -sheets connected by interconnecting loops [7] (Figure 3A). A unique  $\alpha$ -helix is packed underneath one side of the  $\beta$ -sheet. Numerous hydrogen bonds between the  $\beta$ -strands stabilize the framework. The two  $\beta$ -sheets resemble palms and fingers, whereas loops  $\beta$ 12– $\beta$ 13 resemble a thumb-like domain [7]. The  $\beta$ -sheets in the finger domain are almost planar, whereas the  $\beta$ -sheets in the thumb domain are partially twisted to form vertical angles. Long ( $\sim 25$  Å), narrow ( $\sim 4$  Å), and deep ( $\sim 9$  Å) clefts are located between the finger and thumb domains and form the substrate-binding site. The substrate-binding site of GH11 xylanases contains six subsites (Figure 3B), and the catalytic dyad consisting of two Glu residues is located near the center of the substrate-binding pocket. These two Glu residues are positioned facing each other, near the subsite between +1 and –1 (Figure 3B). The narrowest zone of the cleft is located between the conserved Pro residue of the thumb and the conserved aromatic residue (e.g., Trp or Tyr) of the  $\beta$ -strand on the finger domain. Within the substrate-binding cleft, mainly aromatic residues with a few polar residues are located (Figure 3C). The overall architecture, topology, and catalytic cleft residues of GH11 xylanases are widely conserved [7].

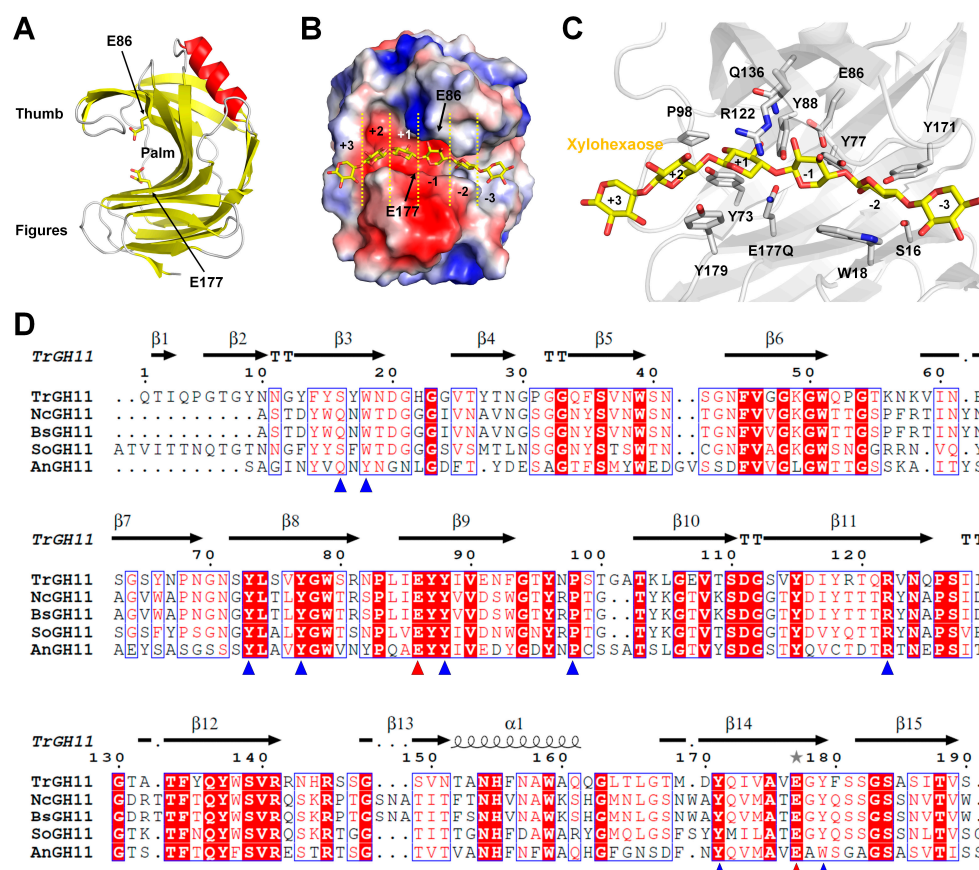


**Figure 3.** GH11 xylanases structure and sequence alignments of GH11 family members: (A) crystal structure of GH11 from *Trichoderma reesei* (PDB code: 1ENX); (B) electrostatic surface of TrGH11 with xylohexose; (C) close-up view of the active site of TrGH11 complexed with xylohexose (PDB code: 4HK8); (D) structure-based sequence alignment of GH11 from *Trichoderma reesei* (TrGH11, UniProt: P36217), *Niallia circulans* (NcGH11, P09850), *Bacillus subtilis* (BsGH11, P18429), *Streptomyces olivaceoviridis* (SoGH11, A0A7G1MBT0), and *Aspergillus niger* (AnGH11, UniProt: P55329).

GH11 from *Trichoderma reesei* is the most structurally studied model among the GH11 family deposited in the PDB (Table 1). The crystal structures of native TrGH11 and its complexes with 4,5-epoxypentyl beta-D-xyloside (PDB code: 1RED), 3,4-epoxybutyl beta-D-xyloside (1REE), 2,3-epoxypropyl beta-D-xyloside (1REF), 2,6-pyridinedicarboxylic acid

(3LGR), xylohexaose (4HK8), and xylotriose (4HK9) have been reported. These structures tentatively provide insights into the substrate recognition or inhibitor of GH11. In particular, the crystal structure of TrGH11 complexed with xylohexaose provides detailed information about substrate recognition (Figure 3C). TrGH11–xylohexaose was able to maintain the xylohexaose complex by replacing the catalytic residue E177 with glutamine. In TrGH11-E177Q, the xylohexaose substrate interacted with residues S16, W18, Y77, Y88, E86, P98, R122, Q136, Y171, Y179, and E177Q (Figure 3C). This complex structure indicates where and how substrates are recognized at the six subsites of GH11. Therefore, it potentially provides insight into protein engineering for amino acids that may be involved in altering GH11 substrate specificities. TrGH11 substrate recognition residues are highly conserved with other GH11 from *Niallia circulans*, *Bacillus subtilis*, *Streptomyces olivoaceoviridis*, and *Aspergillus niger* (Figure 3D). Conversely, TrGH11 S16 and W18 are not absolutely conserved. This result suggests differences in substrate binding and recognition at subsites –2 and –3 for each GH11 (Figure 3D).

### 3. Engineering of GH11 Xylanases for Optimal pH Shifting

Protein engineering involves modifying a protein sequence by substituting, inserting, or deleting nucleotides in the encoding gene to obtain a modified protein that is more suitable for a specific use or purpose. In targeted or site-directed mutagenesis, a specific site within a gene sequence is altered [43]. To shift the optimal pH of GH11 xylanases through engineering, various protein engineering strategies have been performed. These include site-directed mutagenesis [31,32], RD, modeling/site-directed mutagenesis, structural comparison, redesign of electrostatic potential [33], structure analysis [34,35], and bioinformatics- and biostatistics-based approaches (Table 2) [36]. In what follows, we review and discuss important protein engineering achievements in shifting the optimal pH of GH11 xylanases for industrial applications. In particular, we carefully examine the correlation between variant amino acids and functions in engineered GH11 using crystal and modeled structures.

**Table 2.** Engineering of GH11 xylanases for optimal pH shifting.

Enzyme (Wild-Type)	Source	pH Optimum/Stability	Condition	Mutation Approach	Reference
XynA	<i>Bacillus subtilis</i>	pH 6 → 6.5	80 °C	DE (epPCR and DNA shuffling)	[44]
CFXyl3	<i>Cellulomonas flavigena</i>	pH 7 → 6	55 °C	RD	[45]
Xyn5	<i>Dictyoglomus thermophilum</i>	pH 7 → 6	65 °C, alkali-pretreated rice straw	in silico analysis	[10]
TLXynA	<i>Thermomyces lanuginosus</i>	acid tolerance alkali tolerance	65 °C,	RD	[46]
BaxA	<i>Bacillus amyloliquefaciens</i>	pH 6 (broad pH spectrum) → 7 (narrow pH spectrum)	50 °C	DE (EPTD-PCR)	[47]
BCX	<i>Bacillus circulans</i>	pH 6.5 → 5–6	50 °C	RD	[18]
XynB	<i>Thermotoga maritima</i>	pH 5.1 → 5.5, overall pH shift upwards by 0.5	90 °C	RD	[48]
CbX-CD	<i>Caldicellulosiruptor bescii</i>	pH 6.5 → 5.0	70 °C	RD Biomathematics and biostatistics	[36]
XynB	<i>Aspergillus niger</i>	pH 5.0 → 5.5	50 °C	Biomathematics RD	[31]

### 3.1. Directed Evolution (DE)

#### 3.1.1. XynA from *Bacillus subtilis* (BsXynA)

Wide-type BsXynA has optimal hydrolytic activity at 50 °C and pH 6.0 for oat spelt xylan substrate [44]. Ruler et al. engineered BsXynA using the DE method to generate a highly thermostable enzyme [44]. DE via error-prone PCR coupled with a single generation of DNA shuffling has been performed to increase the optimal temperature and obtain thermostable BsXynA variants. Four BsXynA mutants (Q7H, G13R, S22P, and S179C) showed an increase in melting temperature of 20 °C [44]. Using these BsXynA variants as a starting point, further DE experiments were performed to obtain an alkali-tolerant/thermophilic enzyme for application in the pulp industry [49]. DE was performed in the following three stages (Figure 4A): (1) A XynA mutant was produced via error-prone polymerase chain reaction (epPCR) and screened on xylan-containing agar plates at pH 8; (2) the mutants obtained were further mutated through a combination of epPCR and DNA shuffling, and their alkaline pH activity was measured at pH 12.0 and 55 °C; and (3) mutants active at pH 12.0 and 80 °C were generated using the DNA shuffling method. The final engineered BsXynA contained eight mutations (Q7H/G13R/S22P/S31Y/T44A/I51V/I107L/S179C). The optimal activity was at pH 6.5, and the specific activity at pH 8–9 increased three-fold when compared with that of the wild-type BsXynA.

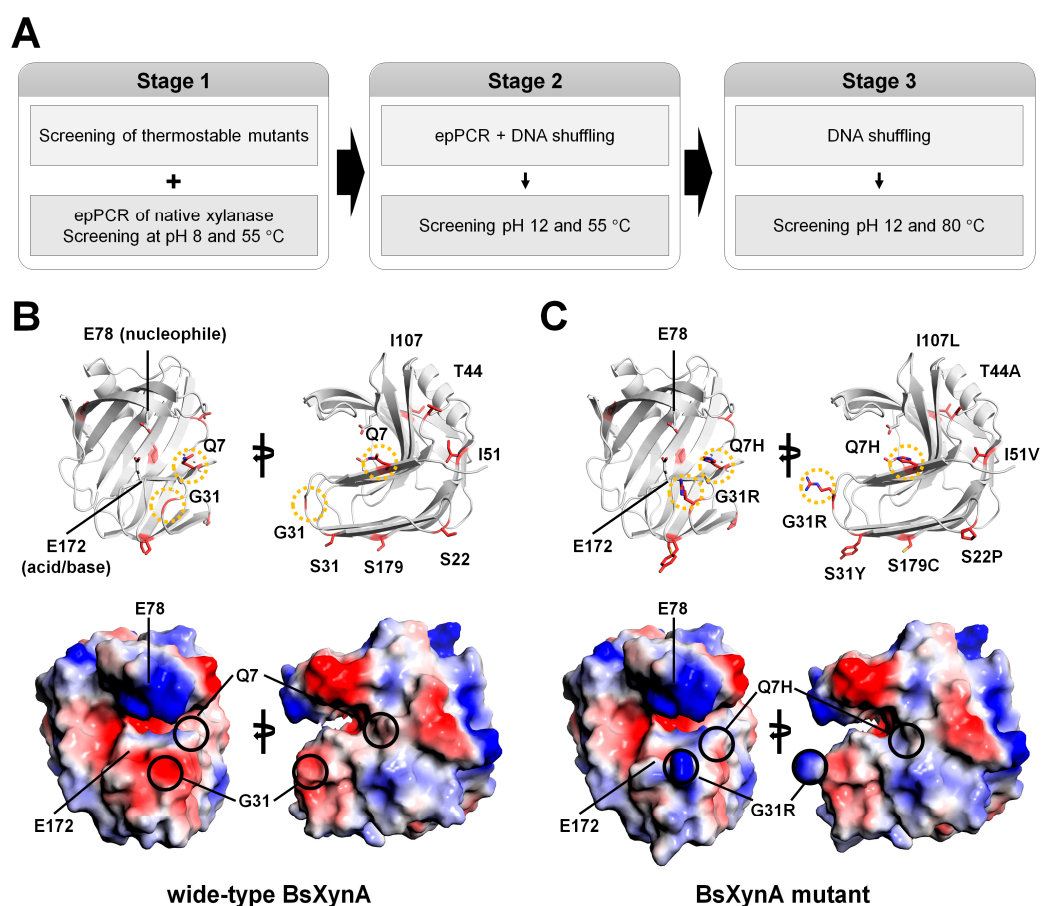


**Figure 4.** BsXynA engineering using the DE method: (A) experimental engineering procedure of BsXynA; (B) crystal structure of wide-type BsXynA (PDB code 1XXN); (C) model structure of BsXynA mutant (Q7H/G13R/S22P/S31Y/T44A/I51V/I107L/S179C).

Considering amino acid characteristics, Q7H, G13R, S22P, S31Y, T44A, and S179C are mutations that can affect protein charge. In contrast, I51V and I107L are neutral mutations as they have the same charge. Based on a previous DE experiment, Q7H, G13R, S22P, and S179C BsXynA mutants have improved thermostability [44]. This result indicates that S31Y, T44A, I151V, and I107L amino acids could affect the optimal pH for xylanase activity.

The crystal structure of wild-type BsXynA (PDB code 1XXN) was used to investigate the structural influence of these amino acids (Figure 4B). The eight mutation sites in the final engineered enzyme were observed to be distributed throughout the GH11 xylanase structure. Among them, amino acids L107 and V51 are located in the hydrophobic interface between the  $\beta$ -sheets. Therefore, I107L and I51V are believed to affect the stability of protein folding rather than pH properties. In contrast, amino acids S22, S31, and S179 are located at the opposite site of the substrate-binding or active sites of BsXynA and may affect the charge state of the protein surface. However, they are not believed to have a direct effect on substrate binding and activity (Figure 4B). Q7 is located near the substrate-binding and active sites, and G13 is located in the finger domain (Figure 4B). This result suggests that mutations at these sites may affect substrate binding or the catalytic reaction. However, the correlation between amino acids that affect pH in the experimental results obtained from enzyme activity and the unique characteristics of these amino acids do not clearly match what affects pH. Considering the comprehensive contents, the eight mutated amino acids were believed to be extensively involved in optimal pH shifting.

To better understand the optimal pH shifting of the BsXynA mutant, the modeling structure of the final engineered BsXynA (Q7H/G13R/S22P/S31Y/T44A/I51V/I107L/S179C) was generated (Figure 4C). The analysis of the electrostatic surface of Q7 and G13 in wild-type BsXynA exhibited negatively charged surfaces, whereas the surface of Q7H and G13R in BsXynA mutant exhibited positively charged surfaces. Overall, the Q7 and G13 residues of BsXynA are involved in thermostability [44] and may affect substrate recognition and enzyme activity.

### 3.1.2. BaxA from *Bacillus amyloliquefaciens*

The xylanase from *B. amyloliquefaciens* expressed in *Escherichia coli* (termed reBaxA) under a *cspA lac* promoter releases xylooligosaccharides from birchwood, beechwood, and oat spelt xylans, yielding xylopentaose, xylotriose, and xyloetraose as their major products, respectively [50]. However, the catalytic activity of reBaxA (2.63 U/mg) was not suitable for practical applications. To improve the catalytic activity of reBaxA for industrial applications, Xu et al. randomly mutagenized reBaxA using the error-prone touchdown (EPTD)-PCR method [47]. PCR products were inserted into the pCold TF vector and then transformed into *E. coli* BL21 (DE3). They obtained an error-prone library of 1463 clones and screened for catalytic activity using a high-throughput screening approach (Figure 5A). The reBaxA50 mutant (S138T), which exhibited higher catalytic activity (9.38 U/mg) than reBaxA, was selected.

For beechwood xylan, the  $K_m$  values of reBaxA50 and reBaxA were 10.50 mg/mL and 13.56 mg/mL, respectively, suggesting that the substrate affinity of the enzyme was improved. The  $V_{max}$  values of reBaxA50 and reBaxA were 42.37  $\mu\text{mol}/\text{min}/\text{mL}$  and 39.52  $\mu\text{mol}/\text{min}/\text{mL}$ , respectively, indicating improved efficiency. The optimal temperature for enzyme activity was 50 °C and 55 °C for reBaxA50 and reBaxA, respectively, and reBaxA50 showed higher activity below 50 °C and above 60 °C. The optimum pH for reBaxA50 and reBaxA was pH 5 and pH 6, respectively. Moreover, reBaxA50 exhibited higher physiological stability than reBaxA under extreme thermal and pH treatments. Overall, S138T in reBaxA50 improved the catalytic activity and thermostability.

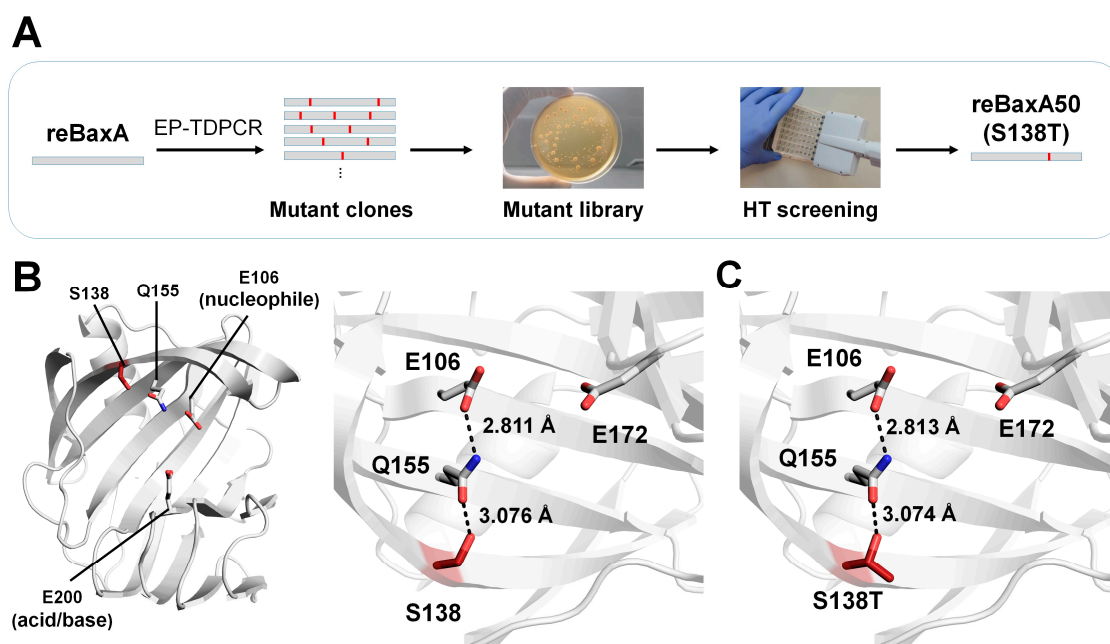


**Figure 5.** Engineering of reBaxA using the DE method: (A) experimental engineering procedure of reBaxA50; (B) crystal structure of reBaxA (PDB code: 2DCY) and close-up view of the interactions between E106, Q155, and S138 residues; (C) model structure of reBaxA50 and close-up view of the interactions of between E106, Q155, and T138 residues.

To understand how S138 affects the catalytic activity, a model structure of reBaxA was generated using the endo-1,4-xylanase A from *B. subtilis* (PDB code: 2DCY) [51] as a template structure. The reBaxA model structure had the typical GH11 xylanase structure. The catalytic residues (Glu106 and Glu200) are located in a substrate-binding cavity between the thumb and finger domains. In the model structures, the Glu106 residues in reBaxA50 and reBaxA form a hydrogen bond with the nitrogen atom of the side chain of Gln155, with distances of 2.811 Å and 2.813 Å, respectively (Figure 5B). The oxygen atom of the side chain of Gln155 forms a hydrogen bond with Thr138 of reBaxA50 and Ser138 of reBaxA in the model structures, with distances of 3.076 Å and 3.074 Å, respectively (Figure 5B). The interactions between Glu106, Gln155, and Ser138 (or Thr138) in their modeling structures in reBaxA50 and reBaxA are almost equal. Conversely, as threonine has one more methyl group than serine, subtle differences in the corresponding site might have an active effect. Xu et al. suggested that the methyl group of Thr138 is directed toward the outside of molecular structure [47], which may enhance the interaction between enzyme and substrate. They also suggested that this is beneficial for the acid catalyst to protonate the substrate and may increase enzymatic activity [47]. They considered that the Thr residue in reBaxA50 created more van der Waals contacts with nearby residues than the Ser in wild-type reBaxA, thereby improving the thermal stability of the xylanase [13]. In contrast, in the case of the modeling structure, as the model is generated depending on the template, it may have provided almost the same results in terms of interaction with Q155 when substituted with S138 and S138T. Therefore, to more accurately understand the pH effect of S138 and S138T, structural analysis using experimental crystal structures will be required.

### 3.2. Rational Engineering

#### 3.2.1. Site-Directed Mutagenesis Engineering of XynB from *Aspergillus niger*

XynB from *A. niger* nl-1 (AnXynB) expressed in *Pichia pastoris* has optimal xylanase activity at pH 5.0 [52]. This protein was engineered to shift the optimal pH toward alkaline pH using site-directed mutagenesis [31]. Positively charged or polar residues near the enzymatic catalytic cleft increase alkalinity [53]. Li et al. compared the amino acid sequence of

AnXynB with those of other xylanases, including *Bacillus* sp. 141M-1, *Bacillus agaradhaerens*, *Bacillus pumilus* A-30, *D. thermophilum* Rt46B.1, *Streptomyces lividans*, *Streptomyces* sp. S38, *Trichoderma reesei*, *Bacillus circulans*, and *Bacillus* sp. D3. They found that eight residues (AASIQGT $\mathbf{A}$ ) in the longer loop located in the substrate-binding area are involved in alkaliphilic adaptation (Figure 6A). In or near the thumb domain, alkaliphilic xylanases contain a conserved Lys residue, whereas acidophilic xylanases contain a charged or non-polar residue (Ile, Val, Glu, Asp, or Gln). The Glu residue in the longer loop of AnXynB was substituted with Lys (AnXynB-Q164K). In addition, the D117 residue located at the edge of the substrate-binding cleft connected via a salt bridge was substituted with Asn, which may have influenced the active site microenvironment.

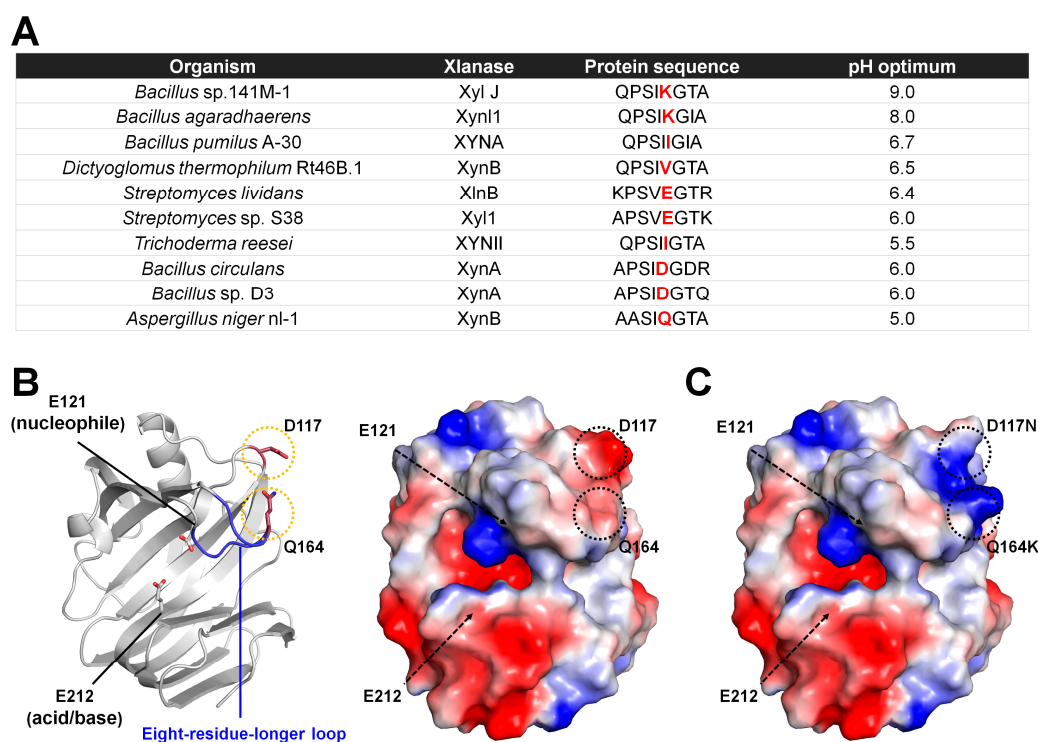


**Figure 6.** AnXynB engineering: (A) comparison of the eight residues involved in alkaliphilic adaptation in the loop sequence of GH11 AnXynB with those in other xylanases; (B) cartoon and electrostatic surface model structures of AnXynB (UniProt: P55330) generated by AlphaFold2; (C) electrostatic surface of modeling structure of AnXynB mutant (D117N and Q164K).

Wild-type AnXynB showed a broad pH profile, with optimal enzyme activity at pH 5.0. AnXynB-164 had a relatively narrow pH profile, with optimal activity near pH 5.0. This result indicates that Q164K does not cause a considerable shift to alkaline pH. XynB-117 showed a relatively narrow pH profile, with an optimum pH of 5.5. This result indicates that D117N does shift the optimal pH of AnXynB. The optimal pH of the double-mutant AnXynB-Q164K/117D was similar to that of the wild type. Therefore, Lys located at the edge of the thumb clearly affected the pH-dependent activity profile. Residual enzyme activity analysis showed that both wild-type AnXynB and AnXynB-164 retained more than 90% of their initial activity after incubation at pH 4.0–10 at 4 °C for 24 h. The residual enzyme activity of AnXynB-117 was higher than that of wild-type AnXynB in the pH range of 5.0–10, except at pH 9.0. In particular, the stability of AnXynB-117 was >30% higher than that of AnXynB at pH 10.0. The optimum temperature analysis of wild-type AnXynB, AnXynB-117, and AnXynB-164 showed that these enzymes were the most active at 45 °C. Compared with AnXynB, AnXynB-164 and AnXynB-117 exhibited higher and lower relative activity in the high-temperature range of 50–60 °C, respectively. The  $K_m/V_{max}$  values of AnXynB, AnXynB-164, and AnXynB-117 were approximately 16.7/188.68, 7.56/112.36,

and 21.42/227.78, respectively. Overall, this study indicated that Q164K, D117N, and Q164K/D117N mutations in the substrate recognition sites, including the xylanase long loop, may be important for the optimal pH or pH stability of xylanase activity. This study engineered GH11 xylanases for shifting the optimal pH and investigated the effects on optimal pH. It also identified amino acid-substituted mutants that affect pH through optimum temperature profiling and  $K_m$  and  $V_{max}$  measurements. These mutants not only affected the pH but also protein stability. These results indicate that protein engineering for the optimal pH shifting of GH11 can alter the optimal pH and other enzymatic properties.

To understand how Q164K and D117N affected the pH activity of AnXynB, model structures of wild-type AnXanB and AnXynB-Q164/D117N generated with AlphaFold was analyzed (Figure 6B). Q164 is located on the eight-residue-longer loop, with the side chain lying on the periphery of subsite  $-2$  or  $-3$  and facing in the opposite direction. However, as the corresponding loop region is a flexible finger-domain region, Q164K could potentially affect substrate recognition at subsites  $-2$  and  $-3$ . When Q164 of AnXynB is converted to Q164K, the negatively charged surface shifts to a positive charge, and the substrate recognition can be affected (Figure 6C). D117N mutant also changes the charge on the protein surface from negative to positive (Figure 6C). However, it has little direct effect on substrate recognition because it is located far from the substrate-binding site.

### 3.2.2. XynA from *Thermomyces lanuginosus*

Thermostable XynA from the filamentous fungus *T. lanuginosus* (TlXynA) exhibits optimum activity at pH 6.0 [54]. To improve pH tolerance, Wu et al. engineered TlXynA based on phylogenetic and amino acid composition analyses [46]. XynJ from *Bacillus* sp. 41M1, halotolerant and acidic xylanase XynC from *Aspergillus kawachii*, and the thermostable TlXynA have optimal pH values of 9.0, 2.0, and 6.0, respectively, and thus they were selected for further study. The study compared the amino acid compositions and surface charges of the crystal structures and found that Arg122, Lys144, and Asp11 were conserved and involved in enzyme function. However, most charged residues were variable, suggesting differences in the enzymatic function of GH11 xylanases. Four positively charged residues (Arg116, Lys119, Arg161, and Arg187) and six non-conserved negatively charged residues (Asn31, Glu36, Glu63, Glu109, Asp143, and Asp157) in TlXynA were mutated to non-polar or uncharged residues (Gln, Thr, Glu, Ser, or Asn). In a mutation study of positive residues of GH11 xylanases, the wild-type and mutants were nearly completely inactive at pH 3.0. However, the TlXynA-R116Q/K119T and TlXynA-R116Q/R161Q mutants showed 40% and 50% of their maximum activity, respectively. This finding suggests that R116, K119, and R116 are critical for resistance to acidic environments. Moreover, in a mutation study of acidic residues of GH11 xylanases, the TlXynA-E63N/E109N, TlXynA-E31S/E63N/E109N, TlXynA-E31S/E63N/E109N/D143S, and TlXynA-E31S/E36S/E63N/E109N/D143S mutants exhibited 86%, 78%, 77%, and 66% of their maximum activity, respectively. In contrast, TlXynA-WT retained approximately 60% of its enzyme activity. This finding indicates that the uncharged state of E63 and E109 is important for generating greater tolerance to an alkaline environment. This mutagenesis study and its biochemical results clearly identified the key residues of GH11 xylanases involved in pH tolerance. Although this study revealed the effect of pH through various mutants, it did not reveal the location of the mutated amino acid within the protein or its effect on the activity.

To understand how the mutation sites in TlXynA affected the pH, the positions of the mutation sites and the surface charge structure of TlXynA are shown using the crystal structure of TlXynA (PDB ID: 1YNA) and modeled mutant structures (Figure 7). Notably, none of the amino acids that affected the pH were located in a position directly involved in the active or substrate-binding sites. R116Q/K119T lies near subsites  $+3$  and  $+2$  in the direction of the thumb domain of the substrate-binding site. R116 and K119 of TlXynA showed a positively charged surface, whereas R116Q/K119T changed the corresponding area to a negatively charged surface. This result indicates that the effect on substrate binding at the subsite  $+2$  and  $+3$  sites in R116Q/K119T may be different

from that in WT. The other mutation sites lie on the surface opposite to the substrate-binding site. In R116Q/R1161Q, the surface charge changed from positive to negative. In the E63N/E109N, TlXynA-E31S/E63N/E109N, TlXynA-E31S/E63N/E109N/D143S, and TlXynA-E31S/E36S/E63N/E109N/D143S mutants, the negative charge surface of TlXynA-WT is replaced by a positively charged surface. These surface charge changes can modify the physical properties or physical characteristics of TlXyn. However, it is difficult to predict how they affect the optimal pH of GH11 because the corresponding position is not around the active site or substrate. In particular, as the structure currently used for mutant position analysis is a modeling structure, there are limitations in explaining the relationship between the active site and substrate-binding site of all mutations. Accordingly, to structurally interpret the effect of mutations more accurately, the analysis should rely on amino acid mutation positions based on actual experimental results rather than modeling results.

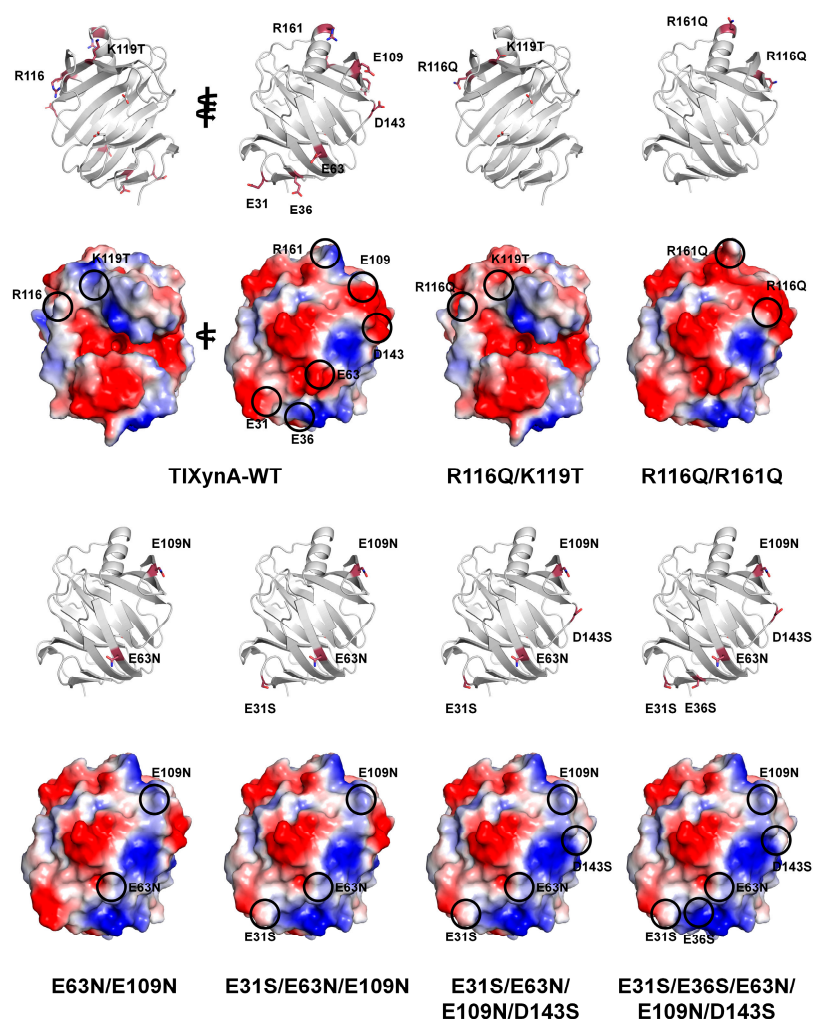


**Figure 7.** Electrostatic surface representation of the model structure of TlXynA and its mutants.

### 3.2.3. Xylanase from *Caldicellulosiruptor bescii*

Evolutionary history reveals a relationship between amino acid sequences of enzymes and their optimal catalytic conditions. Ma et al. developed a strategy for shifting the pH optima of GH11 xylanases using biomathematics and biostatistics [36]. Among more than 1000 GH11 xylanase sequences, 113 sequences of non-redundant and well-characterized enzymes were selected, and a database with annotated pH optima was established. The amino acid sequences were digitized according to their isoelectric point and hydrophathy index. The relationship between the sequences and their pH optima was analyzed using artificial neural networks (ANNs) and the least absolute shrinkage and selection opera-

tor (Lasso) algorithms (Figure 8A). This bioinformatics approach identified six potential residues (Trp21, Thr102, Thr120, Thr137, Ala166, and Asp176) based on the hydrophathy index and eight residues (Asp23, Leu48, Ser56, Trp100, Thr102, Ala108, Ser153, and Gln177) based on the isoelectric point values, related to pH adaptation [36]. Furthermore, the identified residues were mutated in thermophilic xylanase from *C. bescii* (CbX-CD) [36]. The pH activity profiles of wild-type CbX-CD and the mutant enzymes were determined using beechwood xylan as substrate. The optimal pH of wild-type CbX-CD was 6.5. The pH optima for CbX-CD-D176Y and CbX-CD-Q177E showed an acidic shift up to 0.75 units. CbX-CD-S56D and CbX-CD-A166E also exhibited an obvious acidic shift. The pH optima of these mutants were clearly shifted to the acidic side. This result indicates that the mutations altered the pKa values of the catalytic residues rather than simply enhancing the tolerance of the enzyme to an acidic environment. All positive mutants (S56D, A166E, and Q177E) retained a considerable level of catalytic activity, namely 60–90% of the wild-type activity, at their pH optima. No remarkable optimal pH shifts were observed for CbX-CD-L48N, S137I, and S153T.

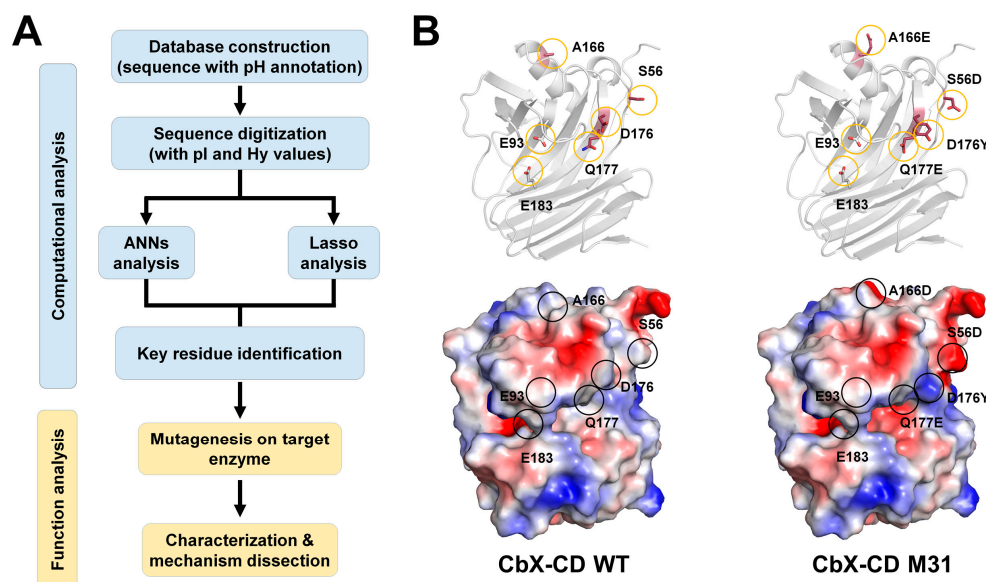


**Figure 8.** Engineering and model structure of CbX-CD: (A) the three-stage rational evolution process of CbX-CD. The original figure was obtained from a previous study [36] and modified; (B) the model structure of the CbX-CD M31 mutant. The positive mutated and catalytic residues are indicated by green and cyan sticks, respectively.

The researchers further explored pH adaptation by combining the positive mutants. The pH activity profiles of four mutants, namely M21 (A166E/Q177E), M22 (S56D/Q177E), M23 (S56D/A166E/Q177E), and M24 (S56D/A166E), were shifted to the acidic side by 1.0 unit. Although they exhibited the same pH shift, each mutant showed a different specific activity. M31 (S56D/A166E/D176Y/Q177E) exhibited a pH optimum of 5.0, which was a 1.5-unit shift toward the acidic side compared with that of the wild type. The M31 mutant maintained approximately 90% maximal activity of the wild type, and at pH 5.0, it exhibited even higher specific activity (3500 U/mg) than the wild-type enzyme (3100 U/mg).

To understand how the positive mutants affect pH adaptation, a model structure of CbX-CD was constructed using Rt46B.1 from *D. thermophilum* (PDB ID IF5J) as a template. The CbX-CD model showed a typical  $\beta$ -jelly roll structure, and the two catalytic residues were Glu183 (acid–base) and Glu93 (nucleophile). The nucleophile Glu93 was surrounded by a series of protonated residues, including Arg50, Tyr84, Tyr95, and Arg128. Glu93 can be stabilized in the deprotonated state through interactions with the protonated residues via hydrogen bonds and salt bridges. These interactions were considered to favor the

nucleophile attack of Glu93 during catalysis. Glu183 was considered to form interactions with Ans46 and Tyr95, providing Glu183 with a suitable pKa to act as an acid–base catalyst.

Ma et al. generated the modeling structure of CbX-CD using Rt46B.1 from *D. thermophilum* as a template (PDB code: IF5J). Model structure analysis showed that S56D, A166E, D176Y, and Q177E residues are far away from catalytic residues. These residues form the hydrogen bond interaction with neighbor molecules (Asp56-Arg88, Glu166-Leu172, Trp176-Lys54, and Glu177-Lys54). To better understand the molecular function of this mutant molecule, in the present study, we also generated the model structure and showed the surface charge of wide-type CbX-CD and its M31 mutant. The most notable change between WT and M31 was the change in protein surface charge (Figure 8C). S56D, A166D, and Q177E formed a negative charge surface compared with WT on the surface of the protein. In contrast, the surface of D176Y changed to a more positive surface. Notably, S56D, Q177E, and D176Y were in close proximity to subsites –2 and –3, which could potentially be involved in substrate recognition. In contrast, A166D was not involved in direct substrate recognition (Figure 8B).

### 3.3. Modification of the N-Terminus of GH11 Xylanases

A GH11 xylanase engineering study showed that introducing a disulfide bridge at the N-terminus of *Thermomyces lanuginosus* GH11 xylanase enhances its thermostability [55]. Furthermore, the substitution of the first six amino acid residues in the N-terminal region of GH11 xylanase from *B. pumilus* improved its thermal stability and structural integrity [56]. Tian et al. engineered the N-terminal region to improve the thermostability of *Cellulomonas flavigena* xylanase CFXyl3 [45]. Notably, this N-terminal modification also affected the pH of the xylanase. *C. flavigena* is an aerobe, mesophilic, gram-positive bacterium that has four xylanases (CFXyl1, CFXyl2, CFXyl3, and CFXyl4). Among them, CFXyl3 belongs to the GH11 family and has an optimal pH of 7. Recombinant CFXyl3 is stable at alkaline pH values (pH 8–12) and moderately thermostable [45]. The N-terminal sequence of CFXyl3 is shorter than those of GH11 xylanases from *Streptomyces*, *Saccharothrix*, *Micromonospora*, and *Herbidospora cretacea* (Figure 9A). To improve its thermostability, the N-terminus of CFXyl3 was substituted with the corresponding region of SyXyn11P, and four hybrid xylanases (EcsXyl1–4) were generated. EcsXyl1–4 had the N-terminal QNVS amino acid sequence of CFXyl3 replaced with the NAQTCLT amino acid sequence, and each of EcsXyl1–4 had a different amino acid substitution in the non-conserved region (Figure 9B).

The purpose of CFXyl3 engineering was to increase its temperature stability by increasing the structural stability of the N-terminus. EcsXyl1–4 showed better thermostability than CFXyl3 but showed different characteristics in terms of optimum temperature and thermal stability. This result indicates that the different amino acid sequences of EcsXyl1–4 have a considerable effect on temperature characteristics. Unlike the variable temperature characteristics, the effects of mutations in EcsXyl1–4 on pH tended to be similar. CFXyl3 had optimal activity at pH 7, whereas EcsXyl1–4 showed optimal activity at pH 6. In terms of pH stability, CFXyl3 was the most stable at pH 7, whereas EcsXyl1–4 were the most stable at pH 6 with reduced stability at pH 7. These findings indicate that structural changes due to amino acid substitutions in the N-terminus potentially affect the optimal pH and pH stability of this xylanase. While EcsXyl1–4 were highly similar in terms of optimal pH activity, they had different levels of stability at alkaline pH.

In the present study, to better understand how the N-terminal mutation affected pH, we compared the structures of CFXyl3 and EcXyl4 using the modeling structure. Modeling resulted in numerous substituted amino acids. Thus, it was not feasible to distinguish which particular amino acid specifically contributed to pH stability. Notably, 1QNVS4 and 27SAV29 at the N-terminal of CFXyl3 are replaced with NAQTCLT and NFC in EcsXyl1–4. Therefore, all EcXyl1–4 form a disulfide bond at the N-terminal located opposite to the activity and substrate binding. This demonstrates the structural rigidity of EcXyl1–4. Most of the substituted amino acids do not directly affect the active site. Instead, they affect the folding of the finger domain or the charge change on the surface opposite to substrate



retained maximal activity at 70–90 °C. Xyn5-CBM2 had seven times lower activity. It had the same optimal pH (7.0) and temperature (90 °C) values as the parental Xyn5. The optimal pH of Xyn5-CBM9, measured at 65 °C, was shifted from 7.0 to  $\leq 5.0$ . However, it maintained relatively high activity even in very alkaline conditions (pH 10.5). Xyn5-CBM9 had increased enzyme activity at high temperatures, approximately four-fold at 90 °C (Figure 10B).

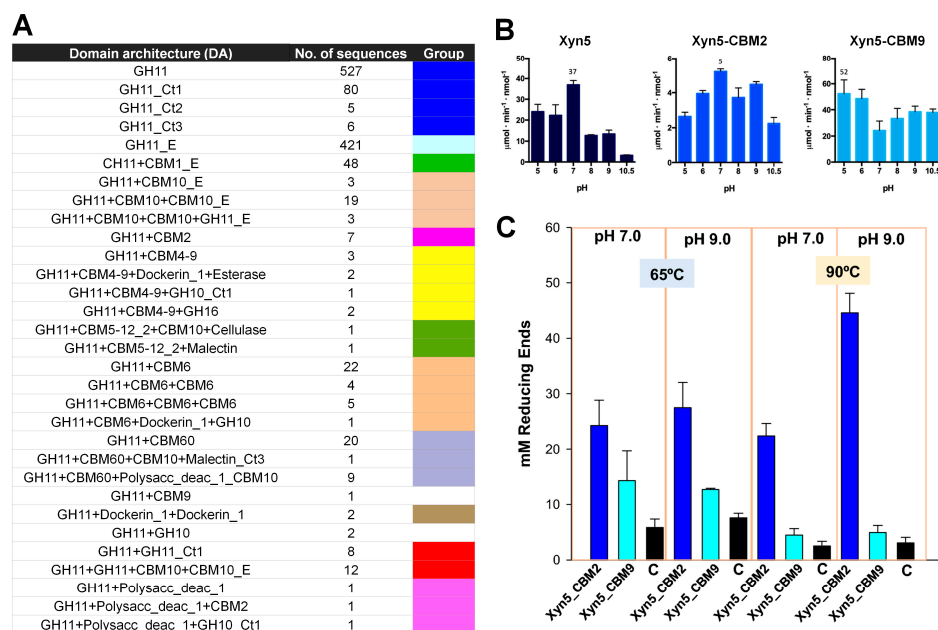


**Figure 10.** CBM-fused xylanases pH profile: (A) domain architectures (DAs) found in GH11 protein sequences in CAZy. Enzymatic activities of Xyn5, Xyn5-CBM2, and Xyn5-CBM9 on purified xylan (B) and rice straw (C). Original figures were obtained from a previous study [10] and modified.

The xylanase activity of Xyn, Xyn5-CBM2, and Xyn5-CBM9 on rice straw, producing soluble sugars through saccharification, was investigated via chromatographic analysis. Xyn, Xyn5-CBM2, and Xyn5-CBM9 produced xylose and oligoxylosides from rice straw. In contrast to the activity on purified xylan, Xyn5-CBM2 had more effective activity on rice straw than Xyn5-CBM9 in all conditions, particularly at 90 °C and pH 9.0 (Figure 10). Taken together, these findings indicate that when a CBM is fused to a xylanase, the pH and temperature properties of the latter change, and different types of CBM may have different characteristics. Accordingly, depending on which CBM is fused to xylanase, the optimal pH or pH stability of the xylanase varies. Xyn5-CBM2 and Xyn5-CBM9 showed contrasting activities on purified xylan and rice straw, indicating that xylanase activity can change depending on the relationship between the CBM and the substrate. This finding highlights the importance of measuring activity based on various substrates when conducting CBM-fused xylanase studies in the future. Although not explicitly mentioned in the study by Talens-Perales et al. [10], the flexibility and stability of fusion proteins vary depending on the length or sequence of the linker used. In the future, it will be interesting to profile xylanase activity according to linker length.

#### 4. Discussion

Xylanases are essential enzymes for energy metabolism in living organisms and are widely used in the food, pulp, and bioenergy industries. In this review, the overall molecular properties of GH11 xylanases and their applications, functions, and structures, as well as notable GH11 xylanase engineering approaches for optimal pH shifting, were reviewed.

GH11 xylanase engineering using DE enabled the optimal pH shifting of XynA from *B. subtilis* and BaxA from *B. amyloliquefaciens*. This approach enables the screening of

their xylanase activity in multiple mutant libraries, which can lead to the identification of functionally improved GH11 xylanases. This method can be used to easily obtain new GH11 mutations that do not exist in nature from various mutant libraries and to create superior mutants through various combinations of amino acid mutations. As numerous mutant libraries are created in this approach, efficient, high-capacity, and fast measurement methods to screen the various mutations in a high-throughput manner are required. Moreover, when mutants are obtained using the DE method, multiple point mutations may be induced simultaneously, necessitating further deconvolution analysis to determine which mutated residue is indeed involved in the pH shift. If the optimal pH shift involves a few mutated amino acids, this residue information can be readily applied to other GH11 xylanases to engineer them for an optimal pH shift. If multiple amino acids affect pH shifting, the residues that directly affect pH can be traced based on structural analysis.

Rational protein engineering for the pH shifting of GH11 xylanases based on previously reported structures or sequences of alkalic or acidic xylanases has also been used. Previous rational engineering studies have indicated that the most influential amino acids in the optimal pH shifting of GH11 xylanases are positively charged residues at substrate recognition sites or substrate-binding sites, including catalytic residues and the finger domain. When a substituted residue is not related to substrate binding and reaction, it affects the charge distribution of the GH11 xylanase surface and may be involved in pH stability rather than optimal pH shifting.

The interaction between the N- and C-terminal regions of GH11 xylanases contributes to protein folding and thermal stability. An amino acid substitution in the N-terminal region, aimed at enabling this region to interact with the C-terminal region and increasing the thermostability of CFXyl3, not only increased thermostability but also affected the optimal pH. Considering the relatively short distance between the active site and the N-terminus of CFXyl3, this finding suggests that the structural stability of the protein affects the optimal pH of GH11 xylanases rather than a specific amino acid site directly affecting pH. Moreover, this result indicates that the optimal pH of GH11 xylanases can change as their thermostability changes. In contrast, other enzyme properties, such as thermostability, can also change their optimal pH value. As the optimal pH achieved through engineering can alter other enzymatic properties of GH11 xylanases, engineered GH11 xylanases should be subjected to enzyme activity optimization experiments. It would be desirable to consider engineered GH11 xylanases as proteins with different characteristics and perform enzyme characterization independently rather than under the same experimental conditions as those used for wild-type xylanases.

According to CAZy data, various CBM-fused GH11 xylanases exist in nature. There are various fusion protein formats, each of which has a unique function in cells. To understand the function of CBM-fused GH11 xylanases, Xyl5 of the extremophilic *D. thermophilum* was fused with CBM2 or CBM5, and their hydrolase activities were measured. Notably, Xyl5-CBM2 and Xyl5-CBM5 showed higher activity than wild-type Xyl5 against rice straw and purified xylan, respectively. This result indicates that the CBM affects substrate-specific activity. Many engineering studies for optimal pH shifting have been performed to increase the activity of GH11 xylanases at a specific pH. Although this review focused on the engineering of GH11 xylanases for pH shifting, it offers promising insights into enhancing the activity of GH11 xylanases at a specific pH. This can be accomplished using the various fusion protein constructs found in the CAZy database, as engineering efforts to optimize the pH of xylanases must align with the fused CBM domains to achieve optimal performance at a given pH value.

In addition to the optimal-pH-shifting-related GH11 xylanase engineering methods reviewed here, point mutations that may affect pH have been structurally analyzed, and amino acids at the corresponding residues have been experimentally verified, demonstrating that they affect pH shifting. However, the mutated residues discussed in this review cannot simply be extrapolated to other GH11 family members. This is because, depending on the degree of amino acid similarity among GH11 family members, different characteris-

tics can be displayed through the interaction of the mutated amino acids with neighboring amino acids. Moreover, protein activity differs among GH11 xylanases depending on the microenvironment, such as the finger domain or substrate-binding cavity.

In addition, to understand the effect of mutant amino acids on the pH shifting of xylanase, we performed a detailed amino acid analysis and surface structure using crystal and model structures. Amino acids in the vicinity of active residues or substrate-binding sites are expected to affect the pH change in terms of potential substrate recognition. However, the direct effect of pH could not be explained, except for one possibility that amino acids at those positions not directly related to GH11 activity or substrate binding generally change the surface charge of proteins. This issue may be attributed to the use of the model structure. For a more accurate structural analysis, future investigations should compare structural differences based on experimental results, such as the actual crystal structure.

In summary, the various approaches and best practices for pH shifting covered in this review will expand our knowledge and provide insights into the engineering of GH11 xylanases for future industrial applications.

**Author Contributions:** Conceptualization, I.J.K. and K.H.N.; investigation, I.J.K. and K.H.N.; data curation, I.J.K. and K.H.N.; writing—original draft preparation, I.J.K., U.T.B. and K.H.N.; writing—review and editing, S.R.K.; visualization, I.J.K. and K.H.N.; funding acquisition, I.J.K. and K.H.N. All authors have read and agreed to the published version of the manuscript.

**Funding:** This work was funded by the National Research Foundation of Korea (NRF) (NRF-2020M3H1A1075314 and NRF-2021R1I1A1A01050838 to K.H.N. and NRF-2022R1I1A1A01072158 to I.J.K.). This work is supported by ProGen (to K.H.N.). This work was carried out with the support of “Cooperative Research Program for Agriculture Science and Technology Development (Project No. PJ01577003)” Rural Development Administration, Republic of Korea.

**Data Availability Statement:** Data generated or analyzed during this study are available from the corresponding author upon reasonable request.

**Conflicts of Interest:** The authors declare no conflict of interest.

## References

1. Bornscheuer, U.; Buchholz, K.; Seibel, J. Enzymatic Degradation of (Ligno)cellulose. *Angew. Chem. Int. Ed.* **2014**, *53*, 10876–10893. [[CrossRef](#)] [[PubMed](#)]
2. Peng, F.; Peng, P.; Xu, F.; Sun, R.-C. Fractional purification and bioconversion of hemicelluloses. *Biotechnol. Adv.* **2012**, *30*, 879–903. [[CrossRef](#)] [[PubMed](#)]
3. Ko, J.K.; Jung, M.W.; Kim, K.H.; Choi, I.-G. Optimal production of a novel endo-acting  $\beta$ -1,4-xylanase cloned from *Saccharophagus degradans* 2-40 into *Escherichia coli* BL21(DE3). *New Biotechnol.* **2009**, *26*, 157–164. [[CrossRef](#)]
4. Cantarel, B.L.; Coutinho, P.M.; Rancurel, C.; Bernard, T.; Lombard, V.; Henrissat, B. The Carbohydrate-Active EnZymes database (CAZy): An expert resource for Glycogenomics. *Nucleic Acids Res.* **2009**, *37*, D233–D238. [[CrossRef](#)]
5. Nguyen, S.T.C.; Freund, H.L.; Kasanjian, J.; Berlemont, R. Function, distribution, and annotation of characterized cellulases, xylanases, and chitinases from CAZy. *Appl. Microbiol. Biotechnol.* **2018**, *102*, 1629–1637. [[CrossRef](#)] [[PubMed](#)]
6. Collins, T.; Gerday, C.; Feller, G. Xylanases, xylanase families and extremophilic xylanases. *FEMS Microbiol. Rev.* **2005**, *29*, 3–23. [[CrossRef](#)]
7. Paës, G.; Berrin, J.-G.; Beaugrand, J. GH11 xylanases: Structure/function/properties relationships and applications. *Biotechnol. Adv.* **2012**, *30*, 564–592. [[CrossRef](#)]
8. Nam, K.H.; Park, S.; Park, J. Preliminary XFEL data from spontaneously grown endo-1,4- $\beta$ -xylanase crystals from *Hypocrea virens*. *Acta Crystallogr. F Struct. Biol. Commun.* **2022**, *78*, 226–231. [[CrossRef](#)]
9. Kim, I.J.; Kim, S.R.; Kim, K.H.; Bornscheuer, U.T.; Nam, K.H. Characterization and structural analysis of the endo-1,4- $\beta$ -xylanase GH11 from the hemicellulose-degrading *Thermoanaerobacterium saccharolyticum* useful for lignocellulose saccharification. *Sci. Rep.* **2023**, *13*, 17332. [[CrossRef](#)]
10. Talens-Perales, D.; Sánchez-Torres, P.; Marín-Navarro, J.; Polaina, J. In silico screening and experimental analysis of family GH11 xylanases for applications under conditions of alkaline pH and high temperature. *Biotechnol. Biofuels* **2020**, *13*, 198. [[CrossRef](#)]
11. Walia, A.; Guleria, S.; Mehta, P.; Chauhan, A.; Parkash, J. Microbial xylanases and their industrial application in pulp and paper biobleaching: A review. *3 Biotech* **2017**, *7*, 11. [[CrossRef](#)] [[PubMed](#)]
12. Sharma, N. Microbial xylanases and their industrial applications as well as future perspectives: A review. *Glob. J. Biol. Agric. Health Sci.* **2017**, *6*, 5–12. [[CrossRef](#)]

13. Viikari, L.; Kantelinen, A.; Sundquist, J.; Linko, M. Xylanases in bleaching: From an idea to the industry. *FEMS Microbiol. Rev.* **1994**, *13*, 335–350. [[CrossRef](#)]
14. Chen, C.-C.; Ko, T.-P.; Huang, J.-W.; Guo, R.-T. Heat- and Alkaline-Stable Xylanases: Application, Protein Structure and Engineering. *ChemBioEng Rev.* **2015**, *2*, 95–106. [[CrossRef](#)]
15. Vahjen, W.; Osswald, T.; Schäfer, K.; Simon, O. Comparison of a xylanase and a complex of non starch polysaccharide-degrading enzymes with regard to performance and bacterial metabolism in weaned piglets. *Arch. Anim. Nutr.* **2007**, *61*, 90–102. [[CrossRef](#)]
16. Lynd, L.R.; Laser, M.S.; Bransby, D.; Dale, B.E.; Davison, B.; Hamilton, R.; Himmel, M.; Keller, M.; McMillan, J.D.; Sheehan, J.; et al. How biotech can transform biofuels. *Nat. Biotechnol.* **2008**, *26*, 169–172. [[CrossRef](#)]
17. Sun, L.; Lee, J.W.; Yook, S.; Lane, S.; Sun, Z.; Kim, S.R.; Jin, Y.-S. Complete and efficient conversion of plant cell wall hemicellulose into high-value bioproducts by engineered yeast. *Nat. Commun.* **2021**, *12*, 4975. [[CrossRef](#)]
18. Pokhrel, S.; Joo, J.C.; Yoo, Y.J. Shifting the optimum pH of *Bacillus circulans* xylanase towards acidic side by introducing arginine. *Biotechnol. Bioprocess Eng.* **2013**, *18*, 35–42. [[CrossRef](#)]
19. Bhardwaj, N.; Kumar, B.; Verma, P. A detailed overview of xylanases: An emerging biomolecule for current and future prospective. *Bioresour. Bioprocess.* **2019**, *6*, 40. [[CrossRef](#)]
20. Hasunuma, T.; Kondo, A. Development of yeast cell factories for consolidated bioprocessing of lignocellulose to bioethanol through cell surface engineering. *Biotechnol. Adv.* **2012**, *30*, 1207–1218. [[CrossRef](#)]
21. Bornscheuer, U.T.; Huisman, G.W.; Kazlauskas, R.J.; Lutz, S.; Moore, J.C.; Robins, K. Engineering the third wave of biocatalysis. *Nature* **2012**, *485*, 185–194. [[CrossRef](#)] [[PubMed](#)]
22. Kan, S.B.J.; Lewis, R.D.; Chen, K.; Arnold, F.H. Directed evolution of cytochrome c for carbon–silicon bond formation: Bringing silicon to life. *Science* **2016**, *354*, 1048–1051. [[CrossRef](#)] [[PubMed](#)]
23. Jumper, J.; Evans, R.; Pritzel, A.; Green, T.; Figurnov, M.; Ronneberger, O.; Tunyasuvunakool, K.; Bates, R.; Žídek, A.; Potapenko, A.; et al. Highly accurate protein structure prediction with AlphaFold. *Nature* **2021**, *596*, 583–589. [[CrossRef](#)] [[PubMed](#)]
24. Dauparas, J.; Anishchenko, I.; Bennett, N.; Bai, H.; Ragotte, R.J.; Milles, L.F.; Wicky, B.I.M.; Courbet, A.; de Haas, R.J.; Bethel, N.; et al. Robust deep learning-based protein sequence design using ProteinMPNN. *Science* **2022**, *378*, 49–56. [[CrossRef](#)] [[PubMed](#)]
25. You, C.; Huang, Q.; Xue, H.; Xu, Y.; Lu, H. Potential hydrophobic interaction between two cysteines in interior hydrophobic region improves thermostability of a family 11 xylanase from *Neocallimastix Patriciarum*. *Biotechnol. Bioeng.* **2010**, *105*, 861–870. [[CrossRef](#)]
26. Zhang, Z.-G.; Yi, Z.-L.; Pei, X.-Q.; Wu, Z.-L. Improving the thermostability of *Geobacillus stearothermophilus* xylanase XT6 by directed evolution and site-directed mutagenesis. *Bioresour. Technol.* **2010**, *101*, 9272–9278. [[CrossRef](#)]
27. Song, L.; Siguier, B.; Dumon, C.; Bozonnet, S.; O'Donohue, M.J. Engineering better biomass-degrading ability into a GH11 xylanase using a directed evolution strategy. *Biotechnol. Biofuels* **2012**, *5*, 3. [[CrossRef](#)]
28. Xiang, L.; Wang, M.; Wu, L.; Lu, Z.; Tang, J.; Zhou, J.; Huang, W.; Zhang, G. Structural insights into xylanase mutant 254RL1 for improved activity and lower pH optimum. *Enzyme Microb. Technol.* **2021**, *147*, 109786. [[CrossRef](#)]
29. Cheng, Y.-S.; Chen, C.-C.; Huang, J.-W.; Ko, T.-P.; Huang, Z.; Guo, R.-T. Improving the catalytic performance of a GH11 xylanase by rational protein engineering. *Appl. Microbiol. Biotechnol.* **2015**, *99*, 9503–9510. [[CrossRef](#)]
30. Kumar, V.; Dangi, A.K.; Shukla, P. Engineering thermostable microbial xylanases toward its industrial applications. *Mol. Biotechnol.* **2018**, *60*, 226–235. [[CrossRef](#)]
31. Zhao, L.; Zhang, X.; Xie, J.; Li, F. Improvement of the Optimum pH of *Aspergillus niger* Xylanase towards an Alkaline pH by Site-Directed Mutagenesis. *J. Microbiol. Biotechnol.* **2015**, *25*, 11–17. [[CrossRef](#)]
32. Qiu, J.; Han, H.; Sun, B.; Chen, L.; Yu, C.; Peng, R.; Yao, Q. Residue mutations of xylanase in *Aspergillus kawachii* alter its optimum pH. *Microbiol. Res.* **2016**, *182*, 1–7. [[CrossRef](#)] [[PubMed](#)]
33. Yang, J.H.; Park, J.Y.; Kim, S.H.; Yoo, Y.J. Shifting pH optimum of *Bacillus circulans* xylanase based on molecular modeling. *J. Biotechnol.* **2008**, *133*, 294–300. [[CrossRef](#)] [[PubMed](#)]
34. Joshi, M.D.; Sidhu, G.; Pot, I.; Brayer, G.D.; Withers, S.G.; McIntosh, L.P. Hydrogen bonding and catalysis: A novel explanation for how a single amino acid substitution can change the pH optimum of a glycosidase. *J. Mol. Biol.* **2000**, *299*, 255–279. [[CrossRef](#)] [[PubMed](#)]
35. Permyakov, E.A.; Bai, W.; Zhou, C.; Zhao, Y.; Wang, Q.; Ma, Y. Structural insight into and mutational analysis of family 11 xylanases: Implications for mechanisms of higher pH catalytic adaptation. *PLoS ONE* **2015**, *10*, e0132834. [[CrossRef](#)]
36. Ma, F.; Xie, Y.; Luo, M.; Wang, S.; Hu, Y.; Liu, Y.; Feng, Y.; Yang, G.-Y. Sequence homolog-based molecular engineering for shifting the enzymatic pH optimum. *Synth. Syst. Biotechnol.* **2016**, *1*, 195–206. [[CrossRef](#)]
37. Sürmeli, Y.; Şanlı-Mohamed, G. Engineering of xylanases for the development of biotechnologically important characteristics. *Biotechnol. Bioeng.* **2023**, *120*, 1171–1188. [[CrossRef](#)]
38. Ardèvol, A.; Rovira, C. Reaction mechanisms in carbohydrate-active enzymes: Glycoside hydrolases and glycosyltransferases. Insights from *ab Initio* quantum mechanics/molecular mechanics dynamic simulations. *J. Am. Chem. Soc.* **2015**, *137*, 7528–7547. [[CrossRef](#)]
39. McCarter, J.D.; Stephen Withers, G. Mechanisms of enzymatic glycoside hydrolysis. *Curr. Opin. Struct. Biol.* **1994**, *4*, 885–892. [[CrossRef](#)]
40. Sinnott, M.L. Catalytic mechanism of enzymic glycosyl transfer. *Chem. Rev.* **2002**, *90*, 1171–1202. [[CrossRef](#)]

41. Nam, K.H.; Lee, W.H.; Rhee, K.H.; Hwang, K.Y. Structural characterization of the bifunctional glucanase-xylanase CelM2 reveals the metal effect and substrate-binding moiety. *Biochem. Biophys. Res. Commun.* **2010**, *391*, 1726–1730. [[CrossRef](#)] [[PubMed](#)]
42. Ishida, T.; Parks, J.M.; Smith, J.C. Insight into the catalytic mechanism of GH11 xylanase: Computational analysis of substrate distortion based on a neutron structure. *J. Am. Chem. Soc.* **2020**, *142*, 17966–17980. [[CrossRef](#)] [[PubMed](#)]
43. Hutchison, C.A.; Phillips, S.; Edgell, M.H.; Gillam, S.; Jahnke, P.; Smith, M. Mutagenesis at a specific position in a DNA sequence. *J. Biol. Chem.* **1978**, *253*, 6551–6560. [[CrossRef](#)] [[PubMed](#)]
44. Ruller, R.; Deliberto, L.; Ferreira, T.L.; Ward, R.J. Thermostable variants of the recombinant xylanase a from *Bacillus subtilis* produced by directed evolution show reduced heat capacity changes. *Proteins* **2007**, *70*, 1280–1293. [[CrossRef](#)] [[PubMed](#)]
45. Tian, W.; Zhang, Z.; Yang, C.; Li, P.; Xiao, J.; Wang, R.; Du, P.; Li, N.; Wang, J. Engineering mesophilic GH11 xylanase from *Cellulomonas flavigena* by rational design of N-terminus substitution. *Front. Bioeng. Biotechnol.* **2022**, *10*, 1044291. [[CrossRef](#)] [[PubMed](#)]
46. Wu, X.; Zhang, Q.; Zhang, L.; Liu, S.; Chen, G.; Zhang, H.; Wang, L. Insights into the role of exposed surface charged residues in the alkali-tolerance of GH11 xylanase. *Front. Microbiol.* **2020**, *11*, 872. [[CrossRef](#)]
47. Xu, X.; Liu, M.-Q.; Huo, W.-K.; Dai, X.-J. Obtaining a mutant of *Bacillus amyloliquefaciens* xylanase A with improved catalytic activity by directed evolution. *Enzyme Microb. Technol.* **2016**, *86*, 59–66. [[CrossRef](#)]
48. Liu, L.; Wang, B.; Chen, H.; Wang, S.; Wang, M.; Zhang, S.; Song, A.; Shen, J.; Wu, K.; Jia, X. Rational pH-engineering of the thermostable xylanase based on computational model. *Process Biochem.* **2009**, *44*, 912–915. [[CrossRef](#)]
49. Ruller, R.; Alponti, J.; Deliberto, L.A.; Zanzporlin, L.M.; Machado, C.B.; Ward, R.J. Concomitant adaptation of a GH11 xylanase by directed evolution to create an alkali-tolerant/thermophilic enzyme. *Protein Eng. Des. Sel.* **2014**, *27*, 255–262. [[CrossRef](#)]
50. Xu, X.; Liu, M.; Dai, X. Expression of recombinant *Bacillus amyloliquefaciens* xylanase A in *Escherichia coli* and potential application in xylan hydrolysis. *BioResources* **2015**, *10*, 4694–4710. [[CrossRef](#)]
51. Miyazaki, K.; Takenouchi, M.; Kondo, H.; Noro, N.; Suzuki, M.; Tsuda, S. Thermal stabilization of *Bacillus subtilis* family-11 xylanase by directed evolution. *J. Biol. Chem.* **2006**, *281*, 10236–10242. [[CrossRef](#)] [[PubMed](#)]
52. Fenel, F.; Zitting, A.-J.; Kantelinen, A. Increased alkali stability in *Trichoderma reesei* endo-1,4- $\beta$ -xylanase II by site directed mutagenesis. *J. Biotechnol.* **2006**, *121*, 102–107. [[CrossRef](#)] [[PubMed](#)]
53. Oh, D.K.; Oh, H.J.; Kim, H.J.; Cheon, J.; Kim, P. Modification of optimal pH in L-arabinose isomerase from *Geobacillus stearothermophilus* for D-galactose isomerization. *J. Mol. Catal. B Enzym.* **2006**, *43*, 108–112. [[CrossRef](#)]
54. Schlacher, A.; Holzmann, K.; Hayn, M.; Steiner, W.; Schwab, H. Cloning and characterization of the gene for the thermostable xylanase XynA from *Thermomyces lanuginosus*. *J. Biotechnol.* **1996**, *49*, 211–218. [[CrossRef](#)]
55. Wang, Y.; Fu, Z.; Huang, H.; Zhang, H.; Yao, B.; Xiong, H.; Turunen, O. Improved thermal performance of *Thermomyces lanuginosus* GH11 xylanase by engineering of an N-terminal disulfide bridge. *Bioresour. Technol.* **2012**, *112*, 275–279. [[CrossRef](#)]
56. Bhat, S.K.; Purushothaman, K.; Kini, K.R.; Gopala Rao Appu Rao, A.R. Design of mutants of GH11 xylanase from *Bacillus pumilus* for enhanced stability by amino acid substitutions in the N-terminal region: An in silico analysis. *J. Biomol. Struct. Dyn.* **2021**, *40*, 7666–7679. [[CrossRef](#)]
57. Drula, E.; Garron, M.-L.; Dogan, S.; Lombard, V.; Henrissat, B.; Terrapon, N. The carbohydrate-active enzyme database: Functions and literature. *Nucleic Acids Res.* **2022**, *50*, D571–D577. [[CrossRef](#)]
58. Nakamura, T.; Mine, S.; Hagihara, Y.; Ishikawa, K.; Ikegami, T.; Uegaki, K. Tertiary structure and carbohydrate recognition by the chitin-binding domain of a hyperthermophilic chitinase from *Pyrococcus furiosus*. *J. Mol. Biol.* **2008**, *381*, 670–680. [[CrossRef](#)]
59. Notenboom, V.; Boraston, A.B.; Kilburn, D.G.; Rose, D.R. Crystal structures of the family 9 carbohydrate-binding module from *Thermotoga maritima* xylanase 10A in native and ligand-bound forms. *Biochemistry* **2001**, *40*, 6248–6256. [[CrossRef](#)]

**Disclaimer/Publisher’s Note:** The statements, opinions and data contained in all publications are solely those of the individual author(s) and contributor(s) and not of MDPI and/or the editor(s). MDPI and/or the editor(s) disclaim responsibility for any injury to people or property resulting from any ideas, methods, instructions or products referred to in the content.